

Deforming the Fredkin spin chain away from its frustration-free point

Khagendra Adhikari* and K. S. D. Beach†

Department of Physics and Astronomy, The University of Mississippi, University, Mississippi 38677, USA

The Fredkin model describes a spin-half chain segment subject to three-body, correlated-exchange interactions and twisted boundary conditions. The model is frustration-free, and its ground state wave function is known exactly. Its low-energy physics is that of a strong xy ferromagnet with gapless excitations and an unusually large dynamical exponent. We study a generalized spin chain model that includes the Fredkin model as a special tuning point and otherwise interpolates between the conventional ferromagnetic and antiferromagnetic quantum Heisenberg models. We solve for the low-lying states, using exact diagonalization and density-matrix renormalization group calculations, in order to track the properties of the system as it is tuned away from the Fredkin point; we also present exact analytical results that hold right at the Fredkin point. We identify a zero-temperature phase diagram with multiple transitions and unexpected ordered phases. The Fredkin ground state turns out to be particularly brittle, unstable to even infinitesimal antiferromagnetic frustration. We remark on the existence of an “anti-Fredkin” point at which all the contributing spin configurations have a spin structure exactly opposite to those in the Fredkin ground state.

I. INTRODUCTION

The construction of a spin-1 quantum spin chain with an exactly solvable ground state [1] and its later generalization to spin- S (for all integer $S > 1$) by Movassagh and Shor [2] have proved to be incredibly fruitful developments. These models describe quantum spins interacting locally in the form of a projector, and they are frustration-free in the sense that it is possible to minimize each term in the Hamiltonian individually. One finds that the unique ground state wave function is an equal-weight superposition of all Motzkin walks [3] (colored for $S > 1$). The resulting structure is similar in spirit to that of the Rokhsar-Kivelson point in the quantum dimer model [4, 5], where all short-range dimer tilings contribute equally in the ground state.

Although the ground state has this exact form, the energy spectrum and other properties are less well known. Analytical work [2, 6] points to some very interesting and unusual behavior. Strong mathematical bounds have been placed on the scaling of the excitation gap and the bipartite entanglement entropy as a function of system size, N . The first surprise is that the system is gapless, as opposed to the more typical situation for exactly solvable spins chains [7, 8]. Second, the excitation gap vanishes polynomially with a dynamical exponent $z > 2$, which implies that these systems cannot be described at low energy by any conformal field theory. (Numerical estimates of the dynamical exponent range from 2.7 to 3.2 [1, 9–11].) Third, the entanglement entropy shows violation of the area law [12], growing as fast as \sqrt{N} .

It was once part of the lore of the field that a unique ground state of a physically plausible (local, translationally invariant) one-dimensional Hamiltonian might violate area law scaling by at most a logarithmic correction. The family of Motzkin spin chains provides an important counterexample. Indeed, systematic frustration-free deformations of the model [13, 14] yield a tunable family of Motzkin-walk wave functions (no

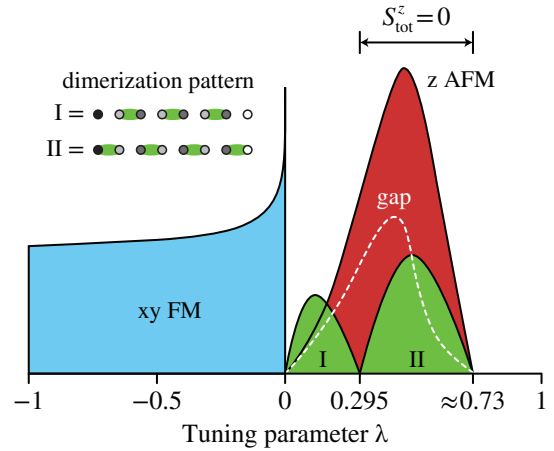


FIG. 1. This diagram summarizes the ground state properties of a spin-half chain with tunable interactions. The system is defined on an open chain with oppositely directed, fully polarized boundary spins. The Fredkin model coincides with $\lambda = 0$; the extremal points describe a conventional nearest-neighbor Heisenberg model with ferromagnetic ($\lambda = -1$) and antiferromagnetic couplings ($\lambda = 1$). The xy ferromagnetism is enhanced as λ increases from -1 , reaching its maximum at $\lambda = 0$. But the Fredkin point serves as the phase boundary. For $\lambda = 0^+$, the ferromagnetism is destroyed, giving way to a gapped, dimerized phase with z-directed Ising antiferromagnetic order. Two different dimer patterns are realized, which exclude (I) and include (II) the boundary spins. The lowest-lying excitations are $S_{\text{tot}}^z = \pm 1$ in character, except in the parameter region coinciding with dimer pattern II, where they are $S_{\text{tot}}^z = 0$.

longer equally weighted) that show a transition between an area-law-compliant phase and an area-law-violating phase in which the entanglement entropy is extensively large ($\sim N$, with maximal violation corresponding to the “rainbow” state proposed in Ref. 15) and the energy gap vanishes exponentially [16].

Systems with comparable character have now been created for odd-half-integer spin, at the cost of allowing for three-site interactions. Salberger and Korepin have proposed a model of

* Electronic address: kadhikar@go.olemiss.edu

† Electronic address: kbeach@olemiss.edu

F_2 , for example, simplify to $U_1 P_{2,3} = P_{2,3}$ and

$$\begin{aligned} P_{1,2} D_3 &= \frac{1}{4} (\mathbb{1} - \sigma_1 \cdot \sigma_2) D_3 \\ &= \frac{1}{4} (\mathbb{1} - \sigma_2^z) D_3 = \frac{1}{2} D_2 D_3. \end{aligned} \quad (5)$$

Hence, the effective Hamiltonian in this limit is

$$H = \sum_{i=3}^{N-2} F_i + P_{2,3} + \frac{D_2 D_3}{2} + P_{N-2, N-1} + \frac{U_{N-2} U_{N-1}}{2}. \quad (6)$$

This formalizes the statement that our model for the length- N chain consists of $N - 2$ active interior spins and two frozen, fully polarized edge spins. In all our numerical work, we have verified that the results we obtain for the ground state and few lowest-lying states are consistent with setting finite field values $\alpha = \beta = 1$ (which is the choice made in Ref. 17).

B. Measuring observables in the ground state

The basic technical challenge for evaluating the properties of the Fredkin model ground state is to generate its $C_{N/2}$ spin configurations of Dyck word form—either exhaustively or via sampling. As it turns out, the Dyck words have a natural lexical ordering, and there are well developed algorithms for systematically stepping through all words of a given length [23, 24]. This is all one needs to make any diagonal or off-diagonal spin measurements: e.g.,

$$\langle \psi_F | \sigma_i^z | \psi_F \rangle = \frac{1}{C_{N/2}} \sum_{\mathcal{D}} \langle \mathcal{D} | \sigma_i^z | \mathcal{D} \rangle \quad (7)$$

and

$$\begin{aligned} &\langle \psi_F | (\sigma_i^+ \sigma_j^- + \sigma_i^- \sigma_j^+) | \psi_F \rangle \\ &= \frac{1}{C_{N/2}} \sum_{\mathcal{D}, \mathcal{D}'} \langle \mathcal{D}' | (\sigma_i^+ \sigma_j^- + \sigma_i^- \sigma_j^+) | \mathcal{D} \rangle \\ &= \frac{1}{C_{N/2}} \sum_{\mathcal{D}} \begin{cases} 1 & \text{if } \downarrow_i \text{ and } \uparrow_j, \\ 1 & \text{if } \uparrow_i \text{ and } \downarrow_j \text{ and Dyck word form} \\ & \text{is preserved after spins are flipped,} \\ 0 & \text{otherwise,} \end{cases} \end{aligned} \quad (8)$$

with $2\sigma^\pm = \sigma^x \pm i\sigma^y$ defining the raising and lowering operators. Nonetheless, exact enumeration of systems much larger than $N = 38$ is impractical because of memory constraints.

A good alternative is to consider a sampling algorithm that generates Dyck words stochastically. Here, we propose such an algorithm. We proceed by defining a height function

$$h_i = \sum_{j=1}^i \sigma_j^z. \quad (9)$$

The set of Dyck word states corresponds to all specifications of spins $\{\sigma_1^z, \sigma_2^z, \dots, \sigma_N^z\}$ such that $h_0 = h_N = 0$ and $h_i \geq 0$ for

all i . In other words, the height function defines a landscape that never drops below the horizon.

We then make the analogy with a biased random walk ($h_{i+1} = h_i \pm 1$) restricted to one-sided excursions ($h_i \geq 0$) and attempt to generate each valid landscape recursively from left to right. The following branching probabilities ensure that each walk starting from $h_0 = 0$ never drops below the horizon and returns to height zero after exactly N steps:

$$\begin{aligned} \text{Prob}(\sigma_{i+1}^z = +1) &= \frac{(h_i + 2)(N - i - h_i)}{2(h_i + 1)(N - i)}, \\ \text{Prob}(\sigma_{i+1}^z = -1) &= \frac{h_i(N - i + h_i + 2)}{2(h_i + 1)(N - i)}. \end{aligned} \quad (10)$$

Note that taking the limit $N \rightarrow \infty$ in these formulas correctly accounts for the infinite-chain limit. Hence we are able to use Monte Carlo techniques to treat finite-size systems or to simulate the thermodynamic limit directly.

The random walk analogy is useful in one other way. It serves as a book-keeping trick for tallying all spin configurations recursively from the left edge rightward. We find that any diagonal spin measurement consisting of a product of σ_i^z taken over some finite range can be solved analytically. For instance, using computer algebra, we find that

$$\begin{aligned} \langle \sigma_1^z \rangle &= 1 \\ \langle \sigma_2^z \rangle = \langle \sigma_3^z \rangle &= \frac{N - 4}{2(N - 1)} \rightarrow \frac{1}{2} \\ \langle \sigma_4^z \rangle = \langle \sigma_5^z \rangle &= \frac{3(N^2 - 10N + 16)}{8(N - 3)(N - 1)} \rightarrow \frac{3}{8} \\ \langle \sigma_6^z \rangle = \langle \sigma_7^z \rangle &= \frac{5(N^3 - 18N^2 + 80N - 96)}{16(N - 5)(N - 3)(N - 1)} \rightarrow \frac{5}{16} \end{aligned} \quad (11)$$

so that each value $\langle \sigma_i^z \rangle$ is given by a ratio of polynomials of order $\lfloor i/2 \rfloor$ in N ; the limiting values shown in Eq. (11) correspond to $N \rightarrow \infty$. We have carried out such computations for a range of site indices $i = 1, 2, \dots, 900$. The results lead us to conclude that the spin profile in the thermodynamic limit (shown in the bottom panel of Fig. 3) has the following closed-form expression:

$$\langle \sigma_i^z \rangle = \frac{1}{22r} \binom{2r}{r} = \frac{2}{\sqrt{\pi(1 + 4r)}} + O(r^{-5/2}), \quad (12)$$

where $r = \lfloor i/2 \rfloor$. The asymptotic form $1/\sqrt{\pi r}$ has previously been derived from an effective theory of the continuum height field; see Eq. (23) of Ref. 11.

We now emphasize an important point regarding the magnetic properties in the ground state. Udagawa and Katsura [18], following the reasoning in Ref. 6, argue that the ‘‘magnetization in the ground state is along the z -direction’’ because $\langle \sigma_i^x \rangle = \langle \sigma_i^y \rangle = 0$. This is somewhat misleading. While it is true that expectation values of σ_i^x and σ_i^y vanish (trivially, by symmetry) in the ground state for any finite-length chain, the more relevant issues are whether there are long-range spin correlations in the ground state (yes, strongly ferromagnetic in the easy xy plane) and whether symmetry-breaking order appears

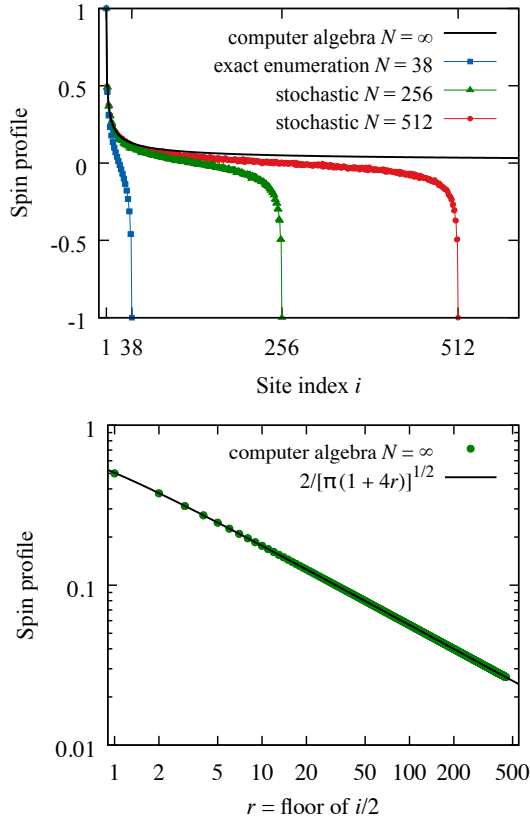


FIG. 3. Top: The z -directed spin profile is shown for various finite system sizes and for the infinite-chain limit. Bottom: Fits of the asymptotic behavior suggest that the spin profile falls off as one over the square root of distance from the edge spin in the infinite-chain limit.

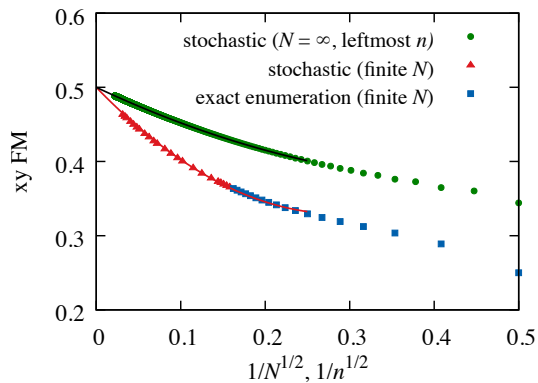


FIG. 4. The order parameter for ferromagnetic alignment in the xy plane, $\sum_{i,j} \langle \sigma_i^+ \sigma_j^- + \sigma_i^- \sigma_j^+ \rangle_N$, is plotted against the inverse square-root system size. The solid red line is a second-order polynomial through the data ($32 < N \leq 1024$). The solid black line is a fit of the same kind, but taken through data for the cumulative xy ferromagnetism, $\sum_{i,j \leq n} \langle \sigma_i^+ \sigma_j^- + \sigma_i^- \sigma_j^+ \rangle_\infty$, measured from one end of the infinite chain. Both extrapolations agree in suggesting that the xy ferromagnetic correlations in the interior of the Fredkin chain are saturated. That is to say, the limits $\langle \sigma_i^z \rangle \rightarrow 0$ and $\langle \sigma_i^x \sigma_j^x + \sigma_i^y \sigma_j^y \rangle \rightarrow 1$ are achieved rapidly as a function of distance from the chain edges.

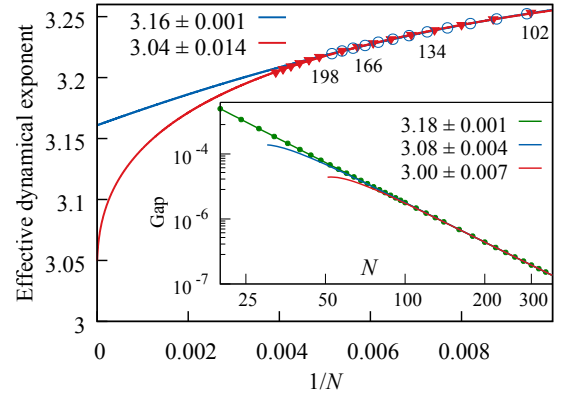


FIG. 5. These data come from density matrix renormalization group calculations, which are described in Sec. III B. In the main panel, the effective dynamical exponent for system size $N + \delta n$, determined from the measured gaps at sizes N and $N + 2\delta n$, is extrapolated to the thermodynamic limit. The first extrapolation (blue, upper curve) is quadratic in $1/N$ (of the form $z_\infty + a_1/N + a_2/N^2$) and fit to data (blue, open circles) on system sizes up to 200 with a finite difference $\delta n = 4$; this is comparable to the analysis carried out in Ref. 11. The second (red, lower curve) allows for a powerlaw form and logarithmic corrections [of the form $z_\infty + (b_0 + b_1 \ln N)/N^\alpha$] and is based on data up to size 260 (red, filled triangles) in steps of 10. The inset shows three fits of the form $\Delta(N) = N^{-z-c_1/N} (d_0 + d_1/N)$, one running through the gap data for all measured system sizes and the other two fit with lower size cutoffs of 150 and 200.

in the thermodynamic limit (no, by virtue of the Mermin-Wagner-Hohenberg theorem [25, 26]).

More specifically, the operator

$$\begin{aligned}
 m_\perp &= \sum_i [(\cos \theta) \sigma_i^x + (\sin \theta) \sigma_i^y] \\
 &= \sum_i (e^{-i\theta} \sigma_i^+ + e^{i\theta} \sigma_i^-),
 \end{aligned} \tag{13}$$

which measures the xy ferromagnetism, satisfies $\langle m_\perp \rangle = 0$, but we can show that $\langle m_\perp^2 \rangle = \sum_{i,j} \langle \sigma_i^+ \sigma_j^- + \sigma_i^- \sigma_j^+ \rangle$ saturates to a finite, nonzero value as $N \rightarrow \infty$. Alternatively—rather than compute the ferromagnetic order parameter over an entire finite-length- N chain—we can compute it over the leftmost n sites of the infinite chain $\sum_{i,j \leq n} \langle \sigma_i^+ \sigma_j^- + \sigma_i^- \sigma_j^+ \rangle_\infty$. Both approaches give extrapolated values that are consistent with fully saturated xy spin correlations in the bulk (see Fig. 4).

This state of affairs is possible because the system supports gapless excitations. These are spin-wave-like in the xy spin plane but have the form of a back-and-forth sloshing of the domain wall when viewed in the z direction. Exactly how the gap vanishes is of special interest. The energy difference between the lowest-lying ($S_z^{\text{tot}} = \pm 1$) excited states and the ($S_z^{\text{tot}} = 0$) ground state scales as $\Delta \sim N^{-z}$, with a dynamical exponent that is unusually large. (This is essentially a jamming effect; the Fredkin term $-F_j$ is a short-bond-shuffle operation, so the evolution is highly constrained.) Movassagh has derived [31] strict upper and lower bounds, $2 < z < 15/2$. The current

best numerical estimate, $z = 3.2$ [11], lies toward the lower end of this range.

Our own numerics are not inconsistent with 3.2, but we stress that a wide range of exponents between 2.8 and 3.3 can be achieved with plausible fitting functions, depending on the precise form of the subleading corrections assumed and the size cutoffs that controls which data are included in the fit. Figure 5 showcases various efforts to extract the dynamical exponent. We consider both (i) $z_{\text{eff}}(N+2) = [\ln \Delta(N+4)/\Delta(N)]/[\ln N/(N+4)]$, extrapolated in various ways to $1/N = 0$, and (ii) a single fit of the full gap data set to the function $\Delta(N) = N^{-z-c_1/N}(d_0 + d_1/N)$. At most, we can say that the correct value of the dynamical exponent lies in the range $3.0 \lesssim z \lesssim 3.2$.

III. GENERALIZED SPIN CHAIN

A. Model

The conventional Heisenberg model involves two-body interactions between neighboring spins, and those interactions are SU(2) invariant. The Fredkin model, on the other hand, makes use of three-body terms that break the spin-rotation-symmetry by picking out a special direction in spin space. We have proposed a tunable model [20, 27] (in the parameter λ) that interpolates between the Fredkin spin chain (at $\lambda = 0$) and the conventional ferromagnetic ($\lambda = -1$) and antiferromagnetic ($\lambda = 1$) quantum Heisenberg models. Recent work has appeared [11] that addresses the ferromagnetic side ($\lambda < 0$) of this model.

The essence of the generalization is to apply to Eq. (2) the operator replacement

$$\begin{aligned} U_i &\rightarrow L_i(\lambda) = \left(\cos \frac{\pi\lambda}{2} \right) U_i - \left(\sin \frac{\pi\lambda}{2} \right) \mathbb{1}, \\ D_i &\rightarrow R_i(\lambda) = \left(\cos \frac{\pi\lambda}{2} \right) D_i - \left(\sin \frac{\pi\lambda}{2} \right) \mathbb{1}. \end{aligned} \quad (14)$$

Hence, the basic three-site operation in the interior is

$$G_i(\lambda) = L_{i-1}(\lambda)P_{i,i+1} + P_{i-1,i}R_{i+1}(\lambda). \quad (15)$$

For $\lambda = 0$, we recover the Fredkin chain, since $L_i(0) = U_i$ and $R_i(0) = D_i$ and hence $G_i(0) = F_i$. Note that any deviation away from this special tuning point breaks the purely Dyck word structure of the ground state, and for $\lambda > 0$ the model is no longer frustration-free.

For $\lambda = \mp 1$, the operators $L_i(\mp 1) = R_i(\mp 1) = \pm \mathbb{1}$ are proportional to the unit matrix, so the model reverts to a ferromagnetic or antiferromagnetic Heisenberg model with conventional two-body exchange interactions:

$$\sum_i G_i(\mp 1) = \pm \sum_i (P_{i,i+1} + P_{i-1,i}) \simeq \pm 2 \sum_i P_{i,i+1}. \quad (16)$$

The operators $L_i(\lambda)$ and $R_i(\lambda)$, defined as linear combinations in Eq. (14), act as dynamical exchange couplings with

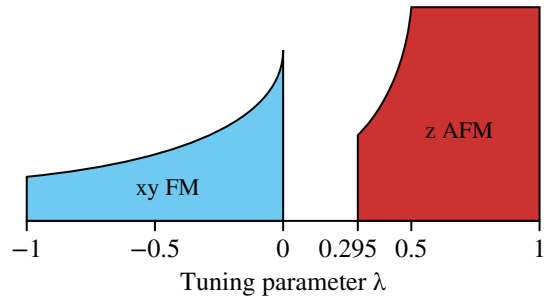


FIG. 6. The phase diagram of the corresponding classical model is drawn based on the measurements of the ground state spin configuration obtained from a global energy optimization. The optimized spin texture shows no direct connection between FM and AFM phases, but instead presents an intervening sequence of spin textures (reminiscent of micro-emulsions [28, 29]) with highly idiosyncratic patterns whose repeat unit grows in steps from 1 to the full system size.

different magnitude and sign depending on the spin-up or spin-down character of the measured spin at site i . As λ increases from 0, the $L_i(\lambda)_{\uparrow\uparrow}$ entry decreases from 1, and $L_i(\lambda)_{\downarrow\downarrow}$ becomes nonzero and increasingly negative. At $\lambda_{c1} = 0.295$, where $2 \tan(\pi\lambda_{c1}/2) = 1$, the spin-up and spin-down entries act with equal magnitude but opposite sign:

$$L_i(\lambda_{c1}) = \frac{1}{\sqrt{5}} \begin{pmatrix} 1 & 0 \\ 0 & -1 \end{pmatrix} = \frac{1}{\sqrt{5}} [U_i - D_i]. \quad (17)$$

As λ is tuned higher still, $L_i(\lambda)_{\uparrow\uparrow}$ continues to decrease. At $\lambda = 0.5$, it vanishes entirely:

$$L_i(0.5) = \frac{1}{\sqrt{2}} \begin{pmatrix} 0 & 0 \\ 0 & -1 \end{pmatrix} = -\frac{1}{\sqrt{2}} D_i. \quad (18)$$

At this parameter value, which we call the anti-Fredkin point, the resulting three-site interaction is similar to that at the Fredkin point, but the sign of the exchange and the filtering at the third adjacent site is reversed. That is to say, whereas the Fredkin model applies a ferromagnetic exchange that acts between a pair of sites whenever a spin up is to its left or a spin down to its right, the anti-Fredkin interaction is antiferromagnetic and acts when there is a spin down to the left and spin up to the right. Equation (15) can also be viewed as a linear superposition of the Fredkin model $G_i(0)$ and the Heisenberg models $G_i(\mp 1)$:

$$G_i(\lambda) = \left(\cos \frac{\pi\lambda}{2} \right) G_i(0) \mp \left(\sin \frac{\pi\lambda}{2} \right) G_i(\mp 1). \quad (19)$$

We note that in the classical version of this model—with σ passing over to a continuous unit vector—the ground state is a fully saturated, z -directed antiferromagnet (z AFM) for $1/2 < \lambda \leq 1$; the antiferromagnetic order is canted when $\lambda_{c1} < \lambda \leq 1/2$; and there is strong, xy -directed ferromagnetism (xy FM) for $\lambda \leq 0$. The phase diagram is depicted in Fig. 6. In Sects. III B and III C, we will show that the quantum version, with spin-half degrees of freedom, looks similar

on the ferromagnetic side ($\lambda \leq 0$)—albeit disordered by U(1) Goldstone modes—but supports a quite different collection of ordered phases on the antiferromagnetic side ($\lambda > 0$).

B. Numerical methods

For a collection of N spin-half objects, the dimension of the Hilbert space is $(2S + 1)^N = 2^N$. Because of this exponential scaling with system size, ED studies are limited to rather small lattices, a few tens of spins at most. This is true even if we take advantage of all the available symmetries and use a Lanczos algorithm to compute just a few of the lowest-lying states. For the model under consideration, we are hindered by the fact that there are only a small number of symmetries that can be exploited.

The Hamiltonian commutes with $S_{\text{tot}}^z = (1/2) \sum_{i=1}^N \sigma_i^z$, the z-component of the total spin, but it does not commute with $S_{\text{tot}}^2 = \mathbf{S}_{\text{tot}} \cdot \mathbf{S}_{\text{tot}} = (1/4) \sum_{i,j} \sigma_i \cdot \sigma_j$, the total spin magnitude. The model possesses a symmetry in which the lattice is inverted and all spins are reversed; in other words, the model is invariant under the transformation

$$\sigma_i^a \Leftrightarrow (\sigma_{L+1-i}^a)^T, \quad (20)$$

for each of $a = x, y, z$. Right at the Fredkin point, we can take advantage of the equivalence classes defined by the number of Dyck-word mismatches, but that does not apply away from $\lambda = 0$. Finally, because the model is defined on an open chain, there is no translational symmetry and hence no well-defined crystal momentum quantum number. So, at best, the Hamiltonian matrix can be block-diagonalized in S_{tot}^z and one additional Z_2 quantum number. This basis-size reduction is not enough to significantly reduce the computational cost. Still, to help guide our investigations, we have generated the full set of energy eigenstates for $N = 12, 14, 16, 18$ over a densely spaced mesh of λ values.

To access larger system sizes, we make use of a DMRG algorithm implemented in the open-source C++ library ITensor [30]. We are mindful of the fact that the high level of entanglement in the vicinity of $\lambda = 0$ requires some additional care. Accordingly, we have employed a very conservative convergence criterion: the DMRG algorithm runs through $7N + 30$ sweeps using an adaptive truncation cutoff at relative error 10^{-12} with maximum bond dimension $10N$. We have verified our DMRG results to near double-precision floating-point accuracy against ED results for $N \leq 18$.

The DMRG computation is carried out for all even lattice sizes up to $N = 80$, over a tight mesh of tuning parameter values $\lambda = -1.000, -0.995, -0.990, \dots, 0.995, 1.000$. The most expensive of those simulations corresponds to 590 sweeps with a maximum bond dimension of 800. The one exception is at $\lambda = 0$, the Fredkin point, where we have made an extra effort to simulate system sizes in steps of 10 up to $N = 350$. Here, the most expensive simulation corresponds to 2520 sweeps with a maximum bond dimension of 3500. Various physical quantities are computed in the ground state as a function of the tuning parameter λ ; i.e., $O(\lambda) = \langle \hat{O} \rangle = \langle \psi_0(\lambda) | \hat{O} | \psi_0(\lambda) \rangle$.

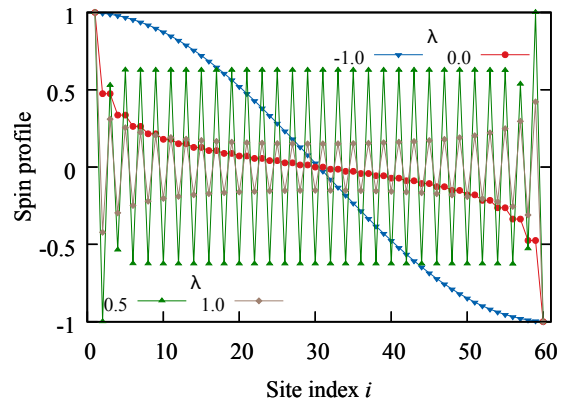


FIG. 7. The spin profile $\langle \sigma_i^z \rangle$ gives the average projection of the spins along the z axis, spatially resolved over sites $i = 1, 2, \dots, N$. Results are given here for system size $N = 60$ and parameter values $\lambda = -1, 0, 0.5$, and 1. Expectation values are computed in the ground state wave function, as determined by DMRG.

These include the spin profile $\langle \sigma_i^z \rangle$, dimer profile $\langle \sigma_i^z \sigma_{i+1}^z \rangle$, dimer order parameter

$$\langle d_{\parallel}^2 \rangle = \frac{1}{N^2} \sum_{i,j=1}^{N-1} (-1)^{i+j} \langle \sigma_i^z \sigma_{i+1}^z \sigma_j^z \sigma_{j+1}^z \rangle, \quad (21)$$

Ising antiferromagnetic order parameter (z AFM)

$$\langle m_{\parallel}^2 \rangle = \frac{1}{N^2} \sum_{i,j=1}^N (-1)^{i+j} \langle \sigma_i^z \sigma_j^z \rangle \quad (22)$$

(as well as its Binder cumulant $Q = 1 - \langle m_{\parallel}^4 \rangle / 3 \langle m_{\parallel}^2 \rangle^2$), and the xy-plane ferromagnetic order parameter (xy FM)

$$\langle m_{\perp}^2 \rangle = \frac{1}{N^2} \sum_{i,j=1}^N \langle \sigma_i^+ \sigma_j^- + \sigma_i^- \sigma_j^+ \rangle. \quad (23)$$

C. Results

At the Fredkin point, the ground state is an equal-amplitude superposition of all spin configurations of Dyck word form. Away from $\lambda = 0$, other non-Dyck-word spin configurations contribute; the Dyck word states still predominate, but they appear with idiosyncratic, λ -dependent amplitudes. Everywhere on the ferromagnetic side of the phase diagram ($\lambda \leq 0$), the single configuration with the largest weight is $((((\dots))))$; on the antiferromagnetic side ($\lambda > 0$), it is $((\dots))$. At two special points, $\lambda_{c1} = 0.295$ and $\lambda = 0.5$, the hard-domain-wall configuration $((((\dots))))$ has no contribution. The change in relative contributions manifests itself in the spin profile, which is shown in Fig. 7.

Because of the incompatible boundary conditions, a ferromagnetic state with full spin-rotation symmetry cannot form at $\lambda = -1$. Instead, the system undergoes a spin flop into

the xy plane. The xy-directed ferromagnetism persists all the way up to $\lambda = 0$. Along the way, the three-body interaction term conspires to produce a strong enhancement of the spin alignment [see Fig. 8(a)].

In the thermodynamic limit, the long-range ferromagnetic correlations die immediately as $\lambda \rightarrow 0^+$, making way for a new phase in which dimer order and z-directed, staggered magnetic order coexist. The numerical data to support this claim are shown in Figs. 8(a)–(d). The $\lambda > 0$ side of the phase diagram exhibits two different patterns of dimerization, which are distinguished by a one-site shift relative to the boundary spins. At large values of the tuning parameter, $0.73 \lesssim \lambda \leq 1$, all order vanishes. This region of the phase diagram is a disordered spin liquid, continuously connected to the ground state of the conventional nearest-neighbor, antiferromagnetic quantum Heisenberg model.

Figure 8(d) reveals the two lobes of dimer order (Fig. 9), corresponding to the patterns plotted in Fig. 10 and illustrated in the top left of Fig. 1. The small lobe on the left side emerges at $\lambda = 0$, takes its maximum value at $\lambda \approx 0.1$, and disappears at $\lambda_{c1} = 0.295$, where all the interior spins are equally correlated with their neighbors. This dimer pattern (I) is weakly coupled to the boundary, and the order is almost independent of the boundary conditions even at small system size. The large lobe on the right appears at $\lambda_{c1} = 0.295$, attains its maximum value at exactly $\lambda = 0.5$, and dies out at $\lambda_{c2} = 0.73$. For this pattern (II), the correlation function that defines the dimer profile is fully saturated ($\langle \sigma_i^z \sigma_{i+1}^z \rangle = -1$ for odd i) at the $\lambda = 0.5$ peak.

Ising antiferromagnetism coexists with the dimerization, forming a dome of z-directed staggered spin order atop the two dimer-ordered lobes in Fig. 1. This gapped, doubly ordered region extends across $0 < \lambda < \lambda_{c2}$ and terminates with second-order phase transitions at either end. We expected to be able to extract the critical exponents for these transitions from data collapse, but the subleading corrections to finite-size scaling turn out to be much too strong for us to do so reliably.

We find that the ground state is unique and belongs to the $S_{\text{tot}}^z = 0$ sector for all values of λ . The lowest-lying excitations are doubly degenerate and $S_{\text{tot}}^z = \pm 1$ everywhere in the phase diagram except in the pattern II dimerized phase, where the excitation is a unique $S_{\text{tot}}^z = 0$ state, and at $\lambda = 0.5$, where the $S_{\text{tot}}^z = 0, \pm 1$ excited states have the same energy. (It must be that those states are pinned together by symmetry, since the three-fold degeneracy holds regardless of system size.) The excitation gap is plotted in Fig. 11. Extrapolation from finite-system data to the $N \rightarrow \infty$ limit suggests that the system is gapped between $\lambda = 0^+$ and $\lambda = \lambda_{c2} = 0.73$, exactly coinciding with the region of dimer order and Ising antiferromagnetism. This is consistent with what we see in the Binder cumulant crossings and in the energy level crossings of the first excited

states (as per Fig. 12).

Various features suggest that $\lambda = 0.5$ is an interesting special tuning point. We have already remarked that it is a point of maximum dimerization strength and that the excitations there are three-fold degenerate. It is also a point where the bipartite entanglement entropy is size-independent, as shown in Fig. 13. Direct investigation of the ground state wave function itself reveals that the structure of the spin configurations that contribute at $\lambda = 0.5$ is similar in spirit to that obtained at $\lambda = 0$. Figure 14 illustrates the connection using the language of the height profile. The underlying cause is that the number of Dyck word mismatches, appropriately defined, is again a good quantum number.

IV. CONCLUSIONS

The proposed model exhibits several interesting phase transitions and highly unusual scaling of the energy gap to the excited states. Figure 1 shows our best estimate of the zero-temperature quantum phase diagram, based on an extrapolation to the thermodynamic limit from our numerical results on finite-size systems.

The ground state evolves smoothly out of the boundary-twisted ferromagnetic state at $\lambda = -1$, and the strength of the xy ferromagnetic correlations increases monotonically to its peak value as λ approaches zero. But the Fredkin state is seemingly not robust: even an infinitesimal amount of antiferromagnetic frustration proves to be completely disruptive. At $\lambda = 0^+$ the ground state changes abruptly. The transition is somewhat unusual, with strong xy ferromagnetic correlations on one side of the transition and vanishing Ising antiferromagnetism and dimer order on the other.

As λ increases from 0^+ , an excitation gap opens up. The Ising antiferromagnetism and dimer order coexist, with the latter switching between two complementary short-range tilings (labeled I and II in Fig. 1) at $\lambda_{c1} = 0.295$. The nature of the excitations in the type-II dimer region is different from everywhere else ($S_{\text{tot}}^z = 0$ rather than $S_{\text{tot}}^z = \pm 1$). All order appears to vanish simultaneously at $\lambda_{c2} = 0.73$. A more precise determination of this rightmost critical value is stymied by strong finite size effects; strictly speaking, we cannot rule out that the Ising antiferromagnetism and type-II dimer order vanish in a closely spaced sequence of transitions, but this seems unlikely.

A most unexpected feature is the presence of another special tuning point at $\lambda = 1/2$, where the ground state wave function mimics (in reverse, for the $N - 2$ interior spins) the Dyck word structure that characterizes the $\lambda = 0$ Fredkin point. Here, however, the state is not an equal-weight superposition. Moreover, it has dimer and staggered Ising order, and its bipartite entanglement entropy is size-independent, suggesting a short-range-entangled, nearly product state.

[1] Sergey Bravyi, Libor Caha, Ramis Movassagh, Daniel Nagaj, and Peter W. Shor, Criticality without Frustration for Quantum

Spin-1 Chains, *Physical Review Letters* **109**, 207202 (2012).
[2] Ramis Movassagh and Peter W. Shor, Supercritical entangle-

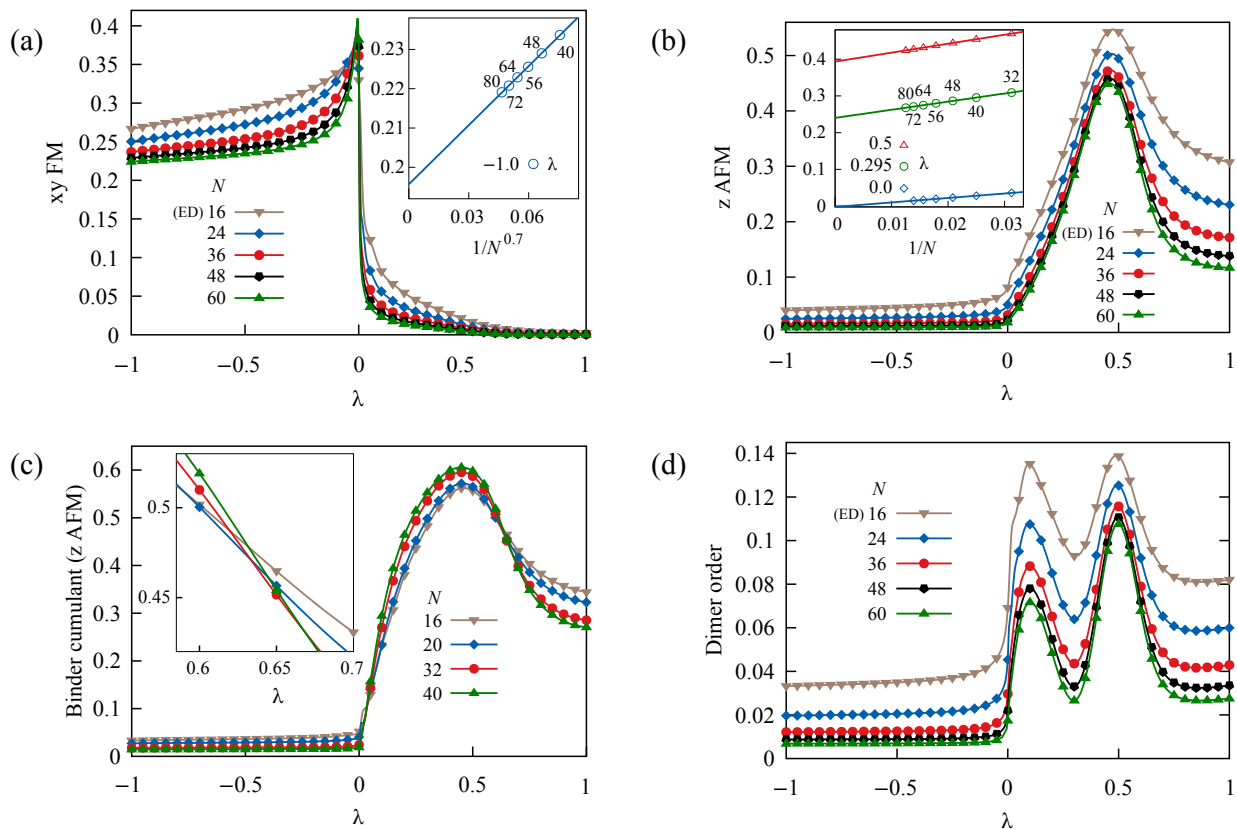


FIG. 8. (a) The xy -directed ferromagnetism, from DMRG and ED calculations, is plotted as a function of λ for various system sizes N . The inset plot in the top right shows the data for $\lambda = -1$ extrapolated versus $1/N^{0.7}$ to $0.196(3)$ in the thermodynamic limit. The numeric labels in the inset plot denote selected values of the system size. (b) The z -directed antiferromagnetism is plotted versus λ for various system sizes N . The maximum value $0.4138(1)$ is obtained at $\lambda = 0.455(2)$. The inset shows extrapolations in $1/N$ for the values $\lambda = 0, 0.295$, and 0.5 . The system has magnetic order in z -direction for $\lambda = 0^+$ in the thermodynamic limit. (c) The Binder cumulant for the Ising antiferromagnetism is plotted as a function of λ for system sizes $N = 16, 20, 32$, and 40 . The crossing points mark the phase boundaries of the region with z -directed staggered order. The inset illustrates the drift of the rightmost crossing point because of strong subleading corrections to finite-size scaling. (d) The dimer order is plotted as a function of λ for various system sizes N . The two lobes represent two phases with distinct patterns of dimerization.

- ment in local systems: Counterexample to the area law for quantum matter, *Proceedings of the National Academy of Sciences* **113**, 13278–13282 (2016).
- [3] R. Donaghey and L. W. Shapiro, Motzkin numbers, *Journal of Combinatorial Theory, Series A* **23**, 291–301 (1977).
- [4] S.A. Kivelson, D.S. Rokhsar, and J.P. Sethna, Topology of the resonating valence-bond state: Solitons and high- T_c superconductivity, *Physical Review B* **35**, 8865(R) (1987).
- [5] Daniel S. Rokhsar and Steven A. Kivelson, Superconductivity and the Quantum Hard-Core Dimer Gas, *Physical Review Letters* **61**, 2376 (1988).
- [6] Ramis Movassagh, Entanglement and correlation functions of the quantum Motzkin spin-chain, *Journal of Mathematical Physics* **58**, 031901 (2017).
- [7] C. K. Majumdar and D. Ghosh, On Next-Nearest-Neighbor Interaction in Linear Chain, *Journal of Mathematical Physics* **10**, 1388 (1969).
- [8] I. Affleck, T. Kennedy, E. H. Lieb, and H. Tasaki, Rigorous results on valence-bond ground states in antiferromagnets, *Physical Review Letters* **59**, 799 (1987).
- [9] L. Dell’Anna, O. Salberger, L. Barbiero, A. Trombettoni, and V. E. Korepin, Violation of cluster decomposition and absence of light cones in local integer and half-integer spin chains, *Physical Review B* **94**, 155140 (2016).
- [10] Xiao Chen, Eduardo Fradkin, and William Witczak-Krempa, Quantum spin chains with multiple dynamics, *Physical Review B* **96**, 180402(R) (2017).
- [11] Xiao Chen, Eduardo Fradkin, and William Witczak-Krempa, Gapless quantum spin chains: multiple dynamics and conformal wavefunctions, *Journal of Physics A: Mathematical and Theoretical* **50**, 464002 (2017).
- [12] J. Eisert, M. Cramer, and M. B. Plenio, Colloquium: Area laws for the entanglement entropy, *Reviews of Modern Physics* **82**, 277 (2010).
- [13] Zhao Zhang, Amr Ahmadain, and Israel Klich, Novel quantum phase transition from bounded to extensive entanglement, *Proceedings of the National Academy of Sciences* **114**, 5142–5146 (2017).
- [14] Zhao Zhang and Israel Klich, Entropy, gap and a multi-parameter deformation of the Fredkin spin chain, *Journal of*

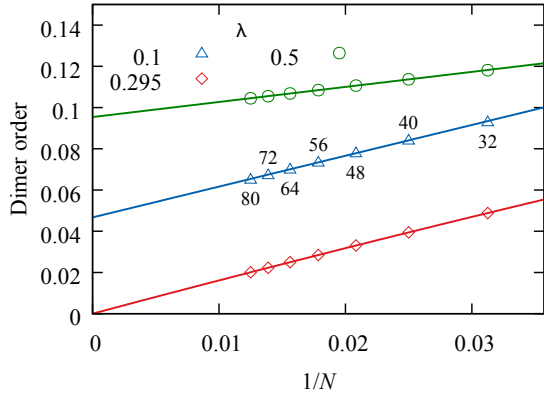


FIG. 9. The dimer order in the thermodynamic limit is determined for parameter values $\lambda = 0.1, 0.295,$ and 0.5 . The values $\lambda = 0.1$ and $\lambda = 0.5$ are chosen to coincide with the two maxima visible in Fig. 8(d). The extrapolated values are $0.0468(2)$ at $\lambda = 0.1$ and $0.0954(1)$ at $\lambda = 0.5$. The dimer order appears to vanish continuously at $\lambda_{c1} = 0.295$.

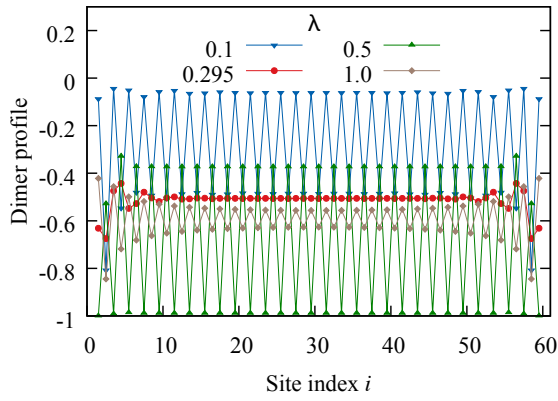


FIG. 10. The dimer profile is the two-point correlation function $\langle \sigma_i^z \sigma_{i+1}^z \rangle$, measured along the spin chain. Results are given here for system size $N = 60$ and parameter values $\lambda = 0.1, 0.295, 0.5,$ and 1 . Expectation values are computed with respect to the ground state wave function, as determined by DMRG. The dimer profile reveals two different pattern of dimerization. The magnitude of the correlation function at its peak value (at $\lambda = 0.5$) is fully saturated (value -1) on alternating bonds.

Physics A: Mathematical and Theoretical **50**, 425201 (2017).

- [15] Giovanni Ramírez, Javier Rodríguez-Laguna, and Germán Sierra, Entanglement over the rainbow, *Journal of Statistical Mechanics: Theory and Experiment* **P06002** (2015).
- [16] Lionel Levine and Ramis Movassagh, The gap of the area-weighted Motzkin spin chain is exponentially small, *Lionel Levine and Ramis Movassagh, Journal of Physics A: Mathematical and Theoretical* **50**, 255302 (2017).
- [17] Olof Salberger and Vladimir Korepin, Fredkin Spin Chain, *arXiv:1605.03842v1* (2016); Entangled spin chain, *Reviews in Mathematical Physics* **29**, 1750031 (2017).
- [18] T. Udagawa and H. Katsura, Finite-size gap, magnetization,

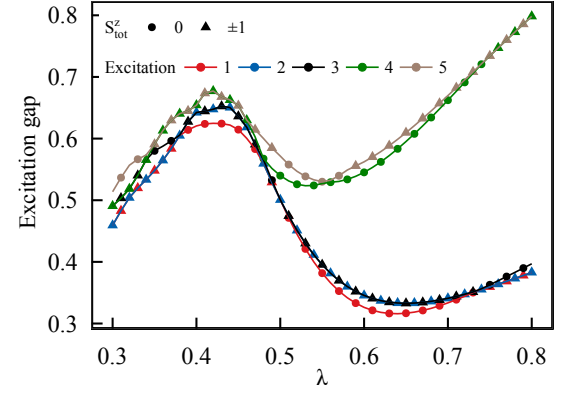
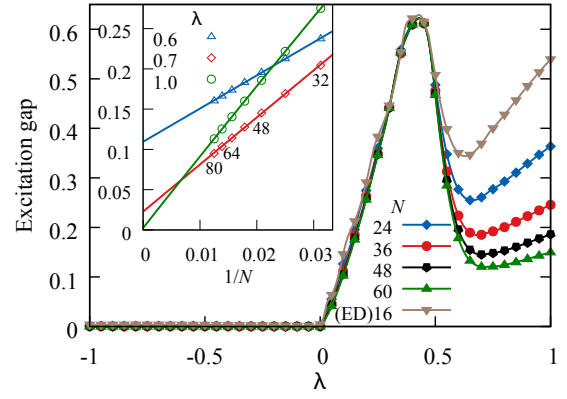


FIG. 11. Top: The excitation gap reaches its maximum value (≈ 0.62) at $\lambda \approx 0.43$. The inset shows the excitation gap versus $1/N$, extrapolated to the thermodynamic limit. The system is clearly gapped for $\lambda = 0.6, 0.7$ and the gapless at $\lambda = 1$, which is consistent with a phase transition at $\lambda_{c2} = 0.73$. In contrast, the excitation gap $\Delta \sim 1/N^z$ on the ferromagnetic side of the phase diagram scales with $z \approx 3$; cf. Figs. 7 and B2 of Ref. 11. Bottom: The data points shown represent the energy difference between each of the first five excited states and the ground state for the $N = 18$ system over a range of λ values in the vicinity of the pattern-II dimerized region. Colors indicate the ranking of the levels, and symbols denote the S_{tot}^z character. Red circles show the $S_{\text{tot}}^z = 0$ states having lowest energy for $\lambda_{c1} < \lambda < \lambda_{c2}$. The next two levels (with $S_{\text{tot}}^z = \pm 1$) come close and touch at exactly $\lambda = 0.5$.

and entanglement of deformed Fredkin spin chain, *Journal of Physics A: Mathematical and Theoretical* **50**, 405002 (2017).

- [19] Pramod Padmanabhan, Fumihiko Sugino, and Vladimir Korepin, Quantum Phase Transitions and Localization in Semigroup Fredkin Spin Chain, *arXiv:1804.00978v1* (2018).
- [20] Khagendra Adhikari and K. S. D. Beach, Deforming the Fredkin spin chain away from its frustration-free point, *APS March Meeting X20.10* (2017).
- [21] The Fredkin model Hamiltonian breaks the Hilbert space into disjoint regions defined by a common number of mismatches from balanced, nested form.
- [22] Away from the chain edges, the terms in Eq. (1) can be regrouped as $\sum_i (U_{i-1} + D_{i+2}) P_{i,i+1}$; this suggests interpreting the Hamiltonian as a correlated Heisenberg model in which the ferromagnetic exchange coupling is sensitive to the configuration

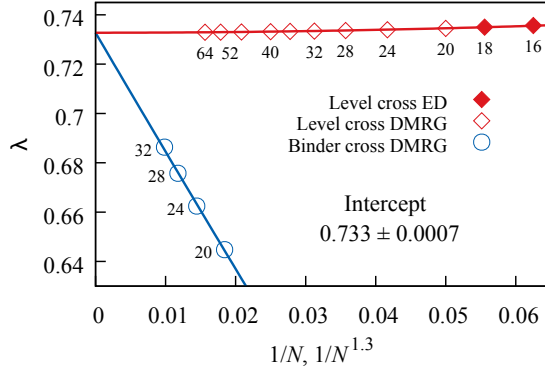


FIG. 12. Shown here are the values of λ at which cross (i) the $S_{\text{tot}}^z = 0$ and $S_{\text{tot}}^z = \pm 1$ first-excited-state energies and (ii) the Binder cumulants for doubled system sizes $N_1 = N$ and $N_2 = 2N$. These are plotted with respect to $1/N$ and $1/N^{1/\nu}$ (using an estimated $\nu = 0.8$ for the correlation length exponent), respectively, and fit with second-order polynomials sharing a common y-axis intercept. The best common intercept is in agreement with our estimated critical point $\lambda_{c2} = 0.73$.

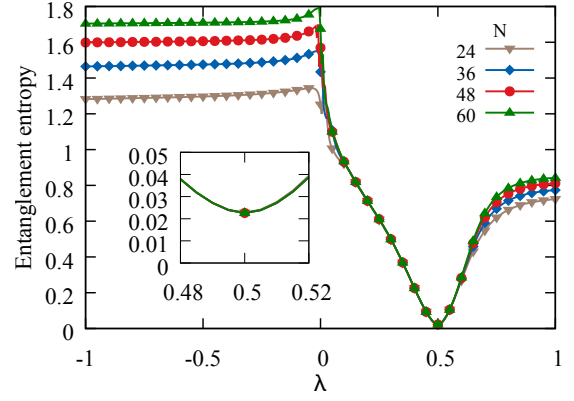


FIG. 13. The von Neumann entanglement energy for a bipartition of the spin chain is given as a function of λ . The peak value and maximum rate of growth with N are located at $\lambda = 0$. For $\lambda = 0.5$, the entanglement entropy appears to be independent of system size, with no corrections to the area law [32].

- of neighboring spins. In contrast to the case of the conventional Heisenberg model, the privileging of the z direction in operators U and D reduces the global spin symmetry from $SU(2)$ to $U(1)$.
- [23] Jörg Arndt, *Matters Computational: Ideas, Algorithms, Source Code*, Springer, Berlin, Heidelberg (2011).
- [24] Donald E. Knuth, *Art of Computer Programming, Volume 2: Seminumerical Algorithms*, 3rd Edition, Addison-Wesley, Boston (1997).
- [25] N. D. Mermin and H. Wagner, Absence of Ferromagnetism or Antiferromagnetism in One- or Two-Dimensional Isotropic Heisenberg Models, *Physical Review Letters* **17**, 1133 (1966); [**17**, 1307(E) (1966)].
- [26] P. C. Hohenberg, Existence of Long-Range Order in One and Two Dimensions, *Physical Review* **158**, 383 (1967).
- [27] Khagendra Adhikari and K. S. D. Beach, A tunable quantum spin chain with three-body interactions, *APS March Meeting H19.10* (2018).
- [28] Boris Spivak and Steven A. Kivelson, Phases intermediate between a two-dimensional electron liquid and Wigner crystal, *Physical Review B* **70**, 155114 (2004).
- [29] Reza Jamei, Steven Kivelson, and Boris Spivak, Universal Aspects of Coulomb-Frustrated Phase Separation, *Physical Review Letters* **94**, 056805 (2005).
- [30] DMRG calculations were performed using the *ITensor* C++ library, developed by E. Miles Stoudenmire and Steven R. White.
- [31] Ramis Movassagh, The gap of Fredkin quantum spin chain is polynomially small, in *Annals of Mathematical Sciences and Applications* **3**, 531 (2018).
- [32] M. B. Hastings, An Area Law for One Dimensional Quantum Systems, *Journal of Statistical Mechanics: Theory and Experiment* **P08024** (2007).

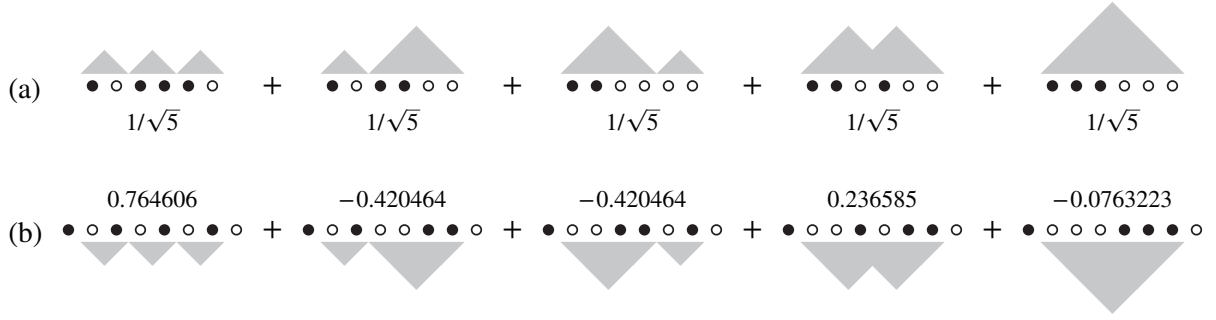


FIG. 14. Shown above are the particular superpositions of spin states that comprise the ground state wave functions for (a) $N = 6$, $\lambda = 0$ and (b) $N = 8$, $\lambda = 1/2$. There is an exact correspondence between the states contributing to the N -site chain at the Fredkin point and those contributing to the $(N+2)$ -site chain at the anti-Fredkin point. At the Fredkin point, the only states contributing are those with a Dyck word structure—which is to say, those having a height profile $h_i = \sum_{j=1}^i \sigma_j^z$ that vanishes at the end points ($h_0 = h_N = 0$) and never drops below the horizon at interior points ($h_i \geq 0$). The structure at the anti-Fredkin point is a mirror-reflection landscape. A modified height function $\tilde{h}_i = \sum_{j=2}^i \sigma_j^z$ vanishes at the end points ($\tilde{h}_1 = \tilde{h}_{N-1} = 0$) and never rises above the horizon ($\tilde{h}_i \leq 0$). This is a consequence of the re-emergence of the number of Dyck word mismatches as a good quantum number for the system.